Supporting Information for: Electroreduction of CO_2/CO to C_2-Products: Process Modeling, Downstream Separation, System Integration, and Economic Analysis

Mahinder Ramdin,[*,†] Bert De Mot,[‡] Andrew R. T. Morrison,[¶] Tom Breugelmans,[‡] Leo J. P. van den Broeke,[†] J. P. Martin Trusler,[§] Ruud Kortlever,[¶] Wiebren de Jong,[¶] Othonas A. Moultos,[†] Penny Xiao,[‖] Paul A. Webley,[⊥] and Thijs J. H. Vlugt[†]

†*Engineering Thermodynamics, Process & Energy Department, Faculty of Mechanical, Maritime and Materials Engineering, Delft University of Technology, Leeghwaterstraat 39, 2628CB Delft, The Netherlands*

‡*Applied Electrochemistry & Catalysis, University of Antwerp, Universiteitsplein 1, 2610 Wilrijk, Belgium*

¶*Large-Scale Energy Storage, Process & Energy Department, Faculty of Mechanical, Maritime and Materials Engineering, Delft University of Technology, Leeghwaterstraat 39, 2628CB Delft, The Netherlands*

§*Imperial College London, South Kensington Campus, London SW7 2AZ, United Kingdom*

‖*Department of Chemical Engineering, University of Melbourne, Victoria 3010, Australia*

⊥*Department of Chemical Engineering, Monash University, Victoria 3800, Australia*

E-mail: m.ramdin@tudelft.nl

S1 Introduction

This supporting information contains:

- Compilation of experimental data of CO_2 reduction to C_2 products (Table S1)
- Compilation of experimental data of CO reduction to C_2 products (Table S2)
- Compilation of experimental data of CO_2 reduction to CO (Table S3)
- Capital and operating cost of the low temperature two-step tandem process (Table S4)
- Capital and operating cost of the high temperature two-step tandem process (Table S5)
- Details of the modeling of the membrane process (Section S2)
- Details of the modeling of the VPSA system for hydrogen, CO, and ethylene separation (Section S3)
- Details of the modeling of the azeotropic distillation of ethanol (Section S4)
- Details of the modeling of extraction and azeotropic distillation of acetic acid (Section S5)
- Estimation of the concentration of ethanol and acetic acid (Section S6)
- Estimation of the loss of CO_2 to (bi)carbonate (Section S7)

Table S1: Compilation of experimental data of CO_2 reduction to C2 products (ethylene, ethanol, and acetic acid).

Reactor	Voltage (V)	CD (mA/cm^2)	FE C_2H_4 (%)	FE EtOH (%)	FE AA (%)	Reference[a]
Flow cell	4	1370	60	15	5	Garcia de Arquer et al.[1]
Flow cell	NS	750	66	11	6	Dinh et al.[2]
Flow cell	2.8	300	57	1	5	De Gregorio et al.[3]
Flow cell	3	300	60	25	2	Hoang et al.[4]
Flow cell	NS	300	51	NS	NS	Vennekotter et al.[5]
Flow cell	3.7	300	38	52	2	Wang et al.[6]
Flow cell	NS	600	80	10	<1	Zhong et al.[7]
Flow cell	2	433	72	18	<1	Chen et al.[8]
Flow cell	NS	320	72	10.5	1.5	Li et al.[9]
Flow cell	NS	1600	65	12	<1	Ma et al.[10]
MEA	3.9	315	66	5	<1	Ozden et al.[11]
Flow cell	NS	670	62	NS	NS	She et al.[12]
Flow cell	NS	300	45	25	<5	Tan et al.[13]
MEA	3.7	580	70	9	8	Wang et al.[14]

[a] In some references, data was only reported in figures. Data extracted from figures are approximated.

Table S2: Compilation of experimental data of CO reduction to C2 products (ethylene, ethanol, and acetic acid).

Reactor	Voltage (V)	CD (mA/cm^2)	FE C_2H_4 (%)	FE EtOH (%)	FE AA (%)	Reference[a]
Flow cell	NS	300	55	17	10	Romero Cuellar et al.[15]
Flow cell	NS	300	45	15	9	Romero Cuellar et al.[16]
Flow cell	3.2	500	40	20	20	Jouny et al.[17]
Flow cell	NS	500	43	14	16	Jouny et al.[18]
Flow cell	NS	1250	65	18	7	Li et al.[19]
Flow cell	NS	200	16	2	48	Luc et al.[20]
MEA	2.5	160	66	6	11	Ozden et al.[21]
Flow cell	NS	200	20	10	40	Ren et al.[22]
MEA	2.3	145	35	4	30	Ripatti et al.[23]
MEA	4	700	28	5	30	Zhu et al.[24]

[a] In some references, data was only reported in figures. Data extracted from figures are approximated.

Table S3: Compilation of experimental data of CO_2 reduction to CO

Reactor configuration	Cell voltage (V)	Current density (mA/cm^2	Faraday efficiency (%)	Reference[a]
Three compartment GDE	6	150	52	Jeanty et al.[25]
Three compartment GDE	3.9	100	40	Duarte et al.[26]
Zero-gap	3	250	>90	Endrodi et al.[27]
Three compartment GDE	NS	150	>90	Dinh et al.[28]
Three compartment GDE	3.5	225	80	Dufek et al.[29]
Three compartment GDE	7.5	300	60	Haas et al.[30]
Three compartment GDE	3	350	>90	Ma et al.[31]
Zero-gap	3.8	300	96	Wang et al.[32]
Zero-gap	3.4	100	70	Salvatore et al.[33]
Micro flow cell	2.2	250	>95	Edwards et al.[34]
Three compartment GDE	NS	200	90	Reinisch et al.[35]
Flow cell	3.0	885	98	Bhargava et al.[36]
Zero-gap	3.5	350	90	Lee et al.[37]
MEA	2.2	240	93	Lee et al.[38]
MEA	2.9	100	99	Kaczur et al.[39]
MEA	3.3	600	93	Liu et al.[40]
Flow cell	2.0	100	99	Verma et al.[41]
Zero-gap	3.4	900	75	Endrodi et al.[42]
Zero-gap	3.2	470	90	Endrodi et al.[43]

[a] In some references, data was only reported in figures. Data extracted from figures are approximated.

Table S4: Capital and operating cost of the low temperature two-step tandem process

Step	CAPEX/\$M	OPEX/\$M/year	CAPEX/%	OPEX/%
CO_2 capture	9.5	1.4	5.2	5.7
CO_2 recycling	8.4	1.3	4.6	5.0
LT CO_2 electrolyzer	85.5	6.4	47.1	25.5
LT CO electrolyzer	59.1	13.3	32.6	52.8
C_2H_4 separation	2.3	0.1	1.3	0.4
CO/H_2 separation	0.5	0.1	0.3	0.4
Ethanol separation	6.7	0.6	3.7	2.5
Acetic acid separation	9.4	1.9	5.2	7.7
Total	181.3	25.2	100.0	100.0

Table S5: Capital and operating cost of the high temperature two-step tandem process

Step	CAPEX/\$M	OPEX/\$M/year	CAPEX/%	OPEX/%
CO_2 capture	9.5	1.4	7.3	5.9
CO_2 recycling	4.1	0.6	3.2	2.5
HT CO_2 electrolyzer	38.2	6.1	29.4	25.2
LT CO electrolyzer	59.1	13.3	45.5	54.9
C_2H_4 separation	2.3	0.1	1.8	0.4
CO/H_2 separation	0.5	0.1	0.4	0.4
Ethanol separation	6.7	0.6	5.2	2.6
Acetic acid separation	9.4	1.9	7.3	8.0
Total	129.8	24.2	100.0	100.0

S2 Modeling of the Membrane Process

For designing the membrane process, the counter-current hollow fiber membrane model of Pettersen and Lien[44] was used. These authors used the Patterson approximation to the logarithmic mean to formulate a simplified multicomponent model in algebraic form to explicitly calculate the permeate molar fraction ($y_{p,i}$) of a component i by:

$$y_{p,i} = \frac{-B_i + \sqrt{B_i^2 - 4A_iC_i}}{2A_i} \tag{S1}$$

where the parameters A_i, B_i, and C_i are functions of the pressure ratio (δ), the molar stage cut (θ), dimensionless permeation factor (R_i), and the feed fraction (z_i):

$$A_i = \frac{\delta}{3}\left(\frac{2\theta}{R} - \delta\right) + \frac{\theta}{3(1-\theta)}\left(\frac{\theta}{R} + \frac{\theta}{12(1-\theta)} - \delta\right) + \left(\frac{\theta}{R}\right)^2 \tag{S2}$$

$$B_i = \frac{z_i}{3}\left(1 + \frac{1}{(1-\theta)}\right)\left(\delta - \frac{\theta}{R}\right) + \frac{\theta z_i}{18(1-\theta)}\left(7 - \frac{1}{(1-\theta)}\right) \tag{S3}$$

$$C_i = \left(\frac{z_i}{6(1-\theta)}\right)^2 (\theta^2 + 12\theta - 12) \tag{S4}$$

with the pressure ratio (δ), the molar stage cut (θ), dimensionless permeation factor (R_i) defined as:

$$\delta = \frac{p_p}{p_f} \tag{S5}$$

$$\theta = \frac{n_p}{n_f} \tag{S6}$$

$$R_i = \frac{aP_ip_f}{n_fl} \tag{S7}$$

where p_p is the permeate pressure, p_f the feed pressure, n_p the molar permeate flow, n_f the molar feed flow, a the membrane area, P_i the permeability coefficient of component i, and l the membrane thickness.

The equations can be solved by applying the following constraint:

$$\sum y_{p,i} = 1 \tag{S8}$$

The selectivities and permeabilities of the different gases in polyamide membranes were taken from Al-Rabiah, see Table S6. For the separation of H_2/CO we have used polyamide A membranes, while for the separation of H_2/C_2H_4 mixtures polyamide B-H membranes were used. Note that hydrogen is the most permeable component in both membranes.

Table S6: Permeabilities and selectivities of polyamide membranes taken from Al-Rabiah.[45]

membrane	H_2/CO	H_2/CH_4	H_2/C_2H_4	H_2/C_2H_6	H_2 permeance (GPU)[a]
polyamide A	100	250	200	1000	100
polyamide B-H	56	125	250	590	500

[a] $\text{GPU} = 10^{-6}\frac{\text{cm}^3(\text{STP})}{\text{cm}^2\cdot\text{s}\cdot\text{cmHg}} = 7.501\text{x}10^{-12}\frac{\text{m}^3(\text{STP})}{\text{m}^2\cdot\text{s}\cdot\text{Pa}}$

An example calculation for the separation of hydrogen and ethylene with polyamide B-H membranes is shown in Figure S1. The calculation is based on a pressure ratio of 10, and a feed concentration of 55% hydrogen and 45% of ethylene. The figure shows that the ethylene purity increases with increasing stage cut, but it is difficult to achieve 99% purity. Furthermore, the capital cost of the membrane process increases with the purity of ethylene.

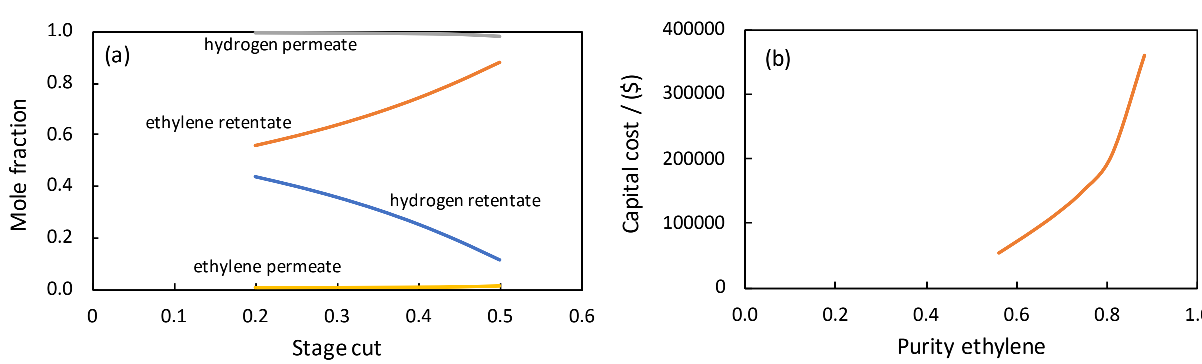

Figure S1: (a) Separation of hydrogen and ethylene with polyamide B-H membranes, and (b) capital cost of the membrane process as a function of the ethylene purity.

S3 Modeling of the VPSA process

The VPSA process for the separation of C_2H_4 and H_2 is presented in Figure S2, and the process simulation was conducted using MINSA (numerical model developed by Melbourne University).[46]

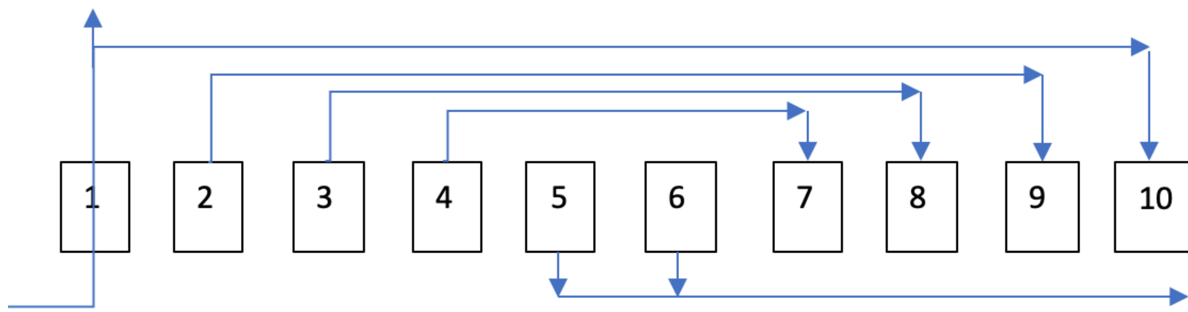

Figure S2: VPSA process design for the separation of ethylene and hydrogen. Step 1, adsorption (10 bar); Step 2 – 4, pressure equalizations; Step 7 – 9, receiving gas for re-pressurization; Step 5, blow down (1 bar); Step 6, vacuum desorption (20 kPa); and Step 10, light component re-pressurization.

The dual-site Langmuir model was used in this process to describe the adsorption capability of activated carbon:

$$q_i(P,T) = \frac{m_i B_{0i}(T) P_i}{1 + \sum B_{0i}(T) P_i} + \frac{n_i D_{0i}(T) P_i}{1 + \sum D_{0i}(T) P_i} \tag{S9}$$

where q_i is the adsorption amount for component i, m_i, n_i, B_{0i} and D_{0i} are Langmuir parameters for component i. The parameters B_{0i} and D_{0i} are correlated as:

$$B_{0i} = b_{0i} \exp\left(\frac{-Q_B}{RT}\right) \tag{S10}$$

$$D_{0i} = d_{0i} \exp\left(\frac{-Q_D}{RT}\right) \tag{S11}$$

where Q_B and Q_D represent the heat of adsorption on two different sites. The dual-site Langmuir parameters are provided in Table S7. The parameters were fitted to the experimental data of Choi et al.[47]

Table S7: Dual-site Langmuir parameters used in the modeling of the VPSA process.

component	m_i (mol/kg)	b_{0i} (1/kPa)	Q_B (J/mol)	n_i (mol/kg)	d_{0i} (1/kPa)	Q_D (J/mol)
C_2H_4	3.4	4.29E-08	29874	3.4	4.29E-08	29874
H_2	6.39	8.76E-06	2900	6.95	1.10E-06	3000

The capital cost of the VPSA unit was estimated based on the units comprising the system (adsorbents, pressure vessels, buffer vessels, valves, vacuum pumps, and compressors). The operating cost is mainly determined by the power consumption of the vacuum pumps and compressors. The capital cost estimate of the VPSA system is provided in Table S8. The prices of different units are taken from Woods and corrected for the size, material type, pressure, and the Chemical Engineering Plant Cost Index. The correlation of Luyben[48] is used to calculate the capital cost of compressors and vacuum pumps:

$$\text{Cost (\$)} = 5840(\text{kW})^{0.82} \tag{S12}$$

The required power (kW) is calculated based on a single stage adiabatic compression assuming an isentropic efficiency of 70%.

Table S8: Capital cost estimation of the VPSA process.

Component	type	Amounts	Price/unit	Cost/M$
Adsorbent	activated carbon	6.2[a]	2000	0.01
Pressure vessels[b]	stainless steel, 1 MPa	5	157860	0.79
Compressor	centrifugal	1	563348	0.56
Vacuum pump	reciprocating	1	120255	0.12
Storage tanks	sphere, 2 bar, s/s, 100 m^3	1	645848	0.65
Valves	butterfly, 10" s/s	27	7685	0.21
Total/ M$				2.34

[a] Tons of activated carbon with a price of $2/kg. Pressure vessels are based on internal diameter of 1.2 m and height of 2 m.

S4 Modeling of Ethanol Separation

The process shown in Figure S3 was modeled in Aspen Plus using the UNIQUAC model. RADFRAC unit blocks have been used to model the distillation columns and the stripper. The optimization of the process is based on the paper of Luyben. The feed (1000 kmol/h) was assumed to contain 10 wt% ethanol with the remainder being water. The ethanol stream was concentrated up to 80 mol% in the ordinary distillation column (ODC). The ODC is optimized by using two design specifications, i.e., the purity of water in the bottom (99.99%) and the concentration of ethanol in the top (80 mol%). The design specifications were met by varying the reflux ratio and the distillate rate. The number of stages and the feed stage were optimized by reducing the reboiler duty using the Model Analysis Tool in Aspen Plus. In a similar way, the azeotropic distillation column (ADC) and the stripper were optimized. For the ADC and stripper, the purity of ethanol and water were set to 99.9% and 99.95%, respectively.

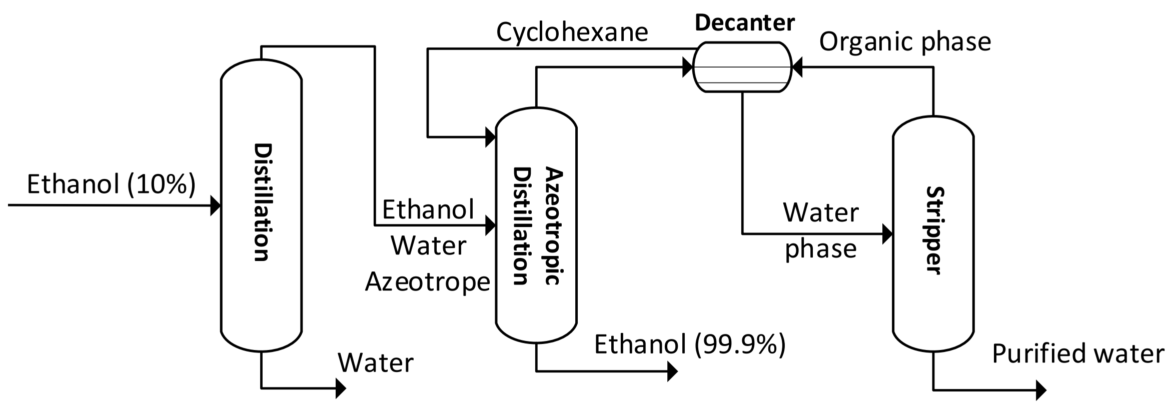

Figure S3: Azeotropic distillation of ethanol with cyclohexane. A feed with 10 wt% ethanol is introduced to a ordinary distillation column (ODC). An ethanol-water azeotropic mixture leaves the ODC as tops, while water is produced as bottoms. The near azeotropic mixture is introduced to the azeotropic distillation column (ADC), where cyclohexane is used as entrainer. Pure ethanol is obtained in the bottom of the ADC, while a cyclohexane-water-ethanol ternary azeotrope is obtained as distillate. This heterogeneous azeotropic mixture is condensed in a decanter into an organic-rich phase and an aqueous phase. The organic-rich phase is recycled to the ADC, while the water phase is sent to the stripper to produce purified water. Steam is used to strip the organics from waste water.

The cyclohexane reflux and the bottoms rate were varied to meet the design specifications of the ADC. The reboiler duty of the stripper was varied to meet the design specification (99.95% water). The optimized parameters for all the columns can be found in Table S9.

Table S9: Azeotropic distillation of ethanol using cyclohexane as entrainer.

Parameter[a]	ODC	ADC	stripper
P / bar	1	2	1
N_{stages}	30	62	11
N_{feed}	20	17	3
organic reflux (kmol/h)	-	70	-
RR (kg/kg) or RD (kW)	1.3	-	600[b]

[a] N_{stages} and N_{feed} are the number of theoretical stages and the feed stage, RR is the reflux ratio, and RD is the reboiler duty. [b] Reboiler duty

The capital and operating cost for processing 1000 kmol/h of feed containing 10 wt% (4.2 mol%) of ethanol are presented in Table xx.

Table S10: Total capital and operating costs for concentrating 10 wt% ethanol to 99.9 wt%.

Capex (M$)	Opex (M$/y)
10.2	1.3

In the electrochemical process, 6.31 mol/s (22.7 kmol/h) of ethanol is produced. If we assume that the concentration of ethanol is 10 wt% (4.2 mol%), then the total molar flow will be 541 kmol/h. We have used the six tenth rule to calculate the capital cost of this flow rate:

$$\frac{\text{Capex}_A}{\text{Capex}_B} = \left(\frac{\text{Flow}_A}{\text{Flow}_B}\right)^a \tag{S13}$$

where a is taken as 0.6. From this, a capital cost of M$7.1 is determined. The operating cost of the process is scaled linearly:

$$\text{Opex}_B = \text{Opex}_A \left(\frac{\text{Flow}_B}{\text{Flow}_A}\right) \tag{S14}$$

which gives an Opex of M$0.7/y.

S5 Modeling of Acetic Acid Separation

The process shown in Figure S4 was modeled in Aspen Plus using the NRTL-HOC model. All model parameters were taken from the Aspen database. The EXTRACT unit block was used for the extractor, and RADFRAC was used for the distillation column and the stripper. The procedure outlined in Shah et al.[49] was used to optimize the hybrid extraction-distillation process. The feed was assumed to contain 20 wt% acetic acid. The extractor was operated at 25 °C and 1 bar. The number of stages and the solvent flow in the extractor were optimized to have an FA recovery of at least 99.0%. For designing extraction columns, the extraction factor (EF) is typically set between 1.5 and 2. The EF is defined as:

$$EF = K_B \frac{S}{F} \tag{S15}$$

where K_B is the partition coefficient in Bancroft coordinates and S/F the solvent to feed ratio.

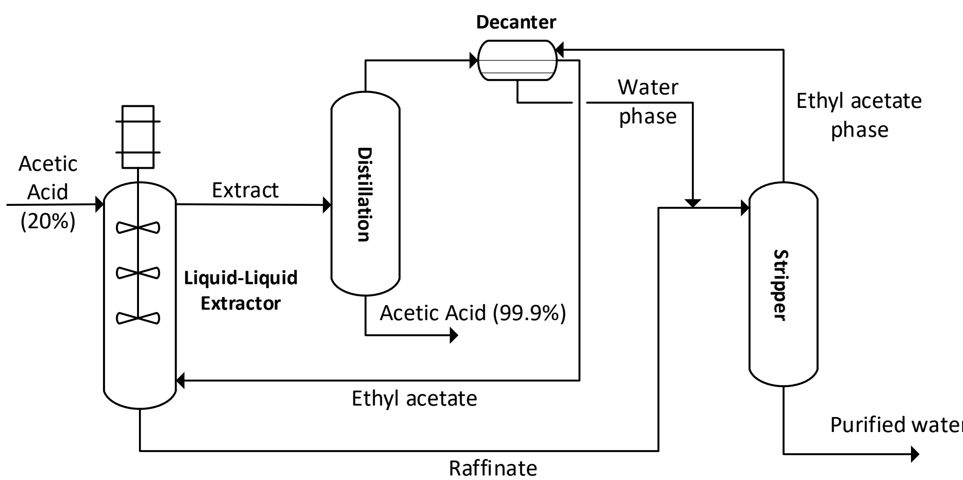

Figure S4: Hybrid extraction-distillation scheme for acetic acid separation. The feed containing 20 wt% acetic acid is introduced at the top of the extractor, while ethyl acetate solvent is fed from the bottom. The extract with acetic acid is fed to the azeotropic distillation column (ADC), which produces nearly pure acetic acid as bottoms. A water–ethyl acetate azeotropic mixture is distilled as tops in the ADC and condensed in a decanter. The organic phase from the decanter is recycled to the extractor, while the aqueous phase is combined with the raffinate and fed to the stripper. Steam is used to strip the organics from the water.

The recovery (R) is defined as:

$$R(\%) = \frac{m_{\mathrm{AA}}^{\mathrm{ext.}}}{m_{\mathrm{AA}}^{\mathrm{F}}} \tag{S16}$$

where $m_{\mathrm{AA}}^{\mathrm{ext.}}$ and $m_{\mathrm{AA}}^{\mathrm{F}}$ are the mass flow of acetic acid in the extract phase and feed, respectively. The optimized parameters for the hybrid extraction-distillation process are provided in Table S11

Table S11: Aspen Plus modeling parameters for the hybrid extraction-distillation process for acetic acid separation.

Parameter[a]	extractor	ADC	stripper
P / bar	1	1	1
N_{stages}	15	30	10
N_{feed}	1	17	1
Solvent flow (kg/h)	25000	-	-
RR (kg/kg) or RD (kW)	-	0.21	1000[b]

[a] N_{stages} and N_{feed} are the number of theoretical stages and the feed stage, RR is the reflux ratio, and RD is the reboiler duty. [b] Reboiler duty

The solvent flow is based on a feed flow of around 10233 kg/h containing 20 wt% of acetic acid. The acetic acid flow is calculated from the current density (500 mA/cm^2) and a Faraday efficiency of 20%, and an electrolyzer area of 7308 m^2. The sizing of the extractor was done using the correlations of Todd.[50] The capital cost of the extractor was then derived using the correlations of Woods,[51] see Table S12. The capital and operating costs of the distillation units were taken directly from Aspen Plus Economic Analyzer and are provided in Table S13.

Table S12: Sizing and costing of the extractor.

Sizing of extractor	
Solute	AA
Feed	water
Solvent	Ethyl acetate
Flow feed kg/hr	10233
Flow solvent kg/hr	25000
Density ρ_c (g/cm^3)	1
Density ρ_d (g/cm^3)	0.90
Flow Qc (m^3/h)	10.233
Flow Qd (m^3/h)	27.78
Ratio Qc/Qd	0.4
Constant B	0.4
Viscosity μ_c (poise)	0.01
Surface tension (dyne/cm)	30
$\Delta\rho$	0.1
Qd$^{0.5}$	5.27
$(\mu_c/\sigma)^{0.088}$	0.49
$(\rho_c^2/\mu_c\Delta\rho)^{0.138}$	2.59
Diameter D (m)	1.52
Theo. stages n	15
Height contact L (m)	17.4
Height clarif. Z (m)	3.7
Total height H (m)	21.1
Traffic flow m^3/m^2 hr	48.4
Capital cost estimation	
ref. FOB cost ($)	380000
$H * D^{1.5}$	39.54
ref $H * D^{1.5}$	10
n	0.66
L+M*	2
L/M	0.48
Cost FOB ($)	941586
L+M ($)	1883172
ref CEPCI	1000
CEPCI 2020	596.2
PM ($)	2118568
BM ($)	2965995
TM at CEPCI = 1000 ($)	4448993
Total M$	2.7

Table S13: Aspen Plus modeling parameters for the hybrid extraction-distillation process for acetic acid separation.

Unit	Capex (M$)	Opex (M$/y)
ADC and stripper	5.7	1.6
Extractor	2.7	0[a]
Total	8.4	1.6

[a] Operating cost of the extractor was neglected, since this is typically very small compared to the cost of the distillation units (ADC and stripper)

S6 Concentration of Ethanol and Acetic Acid

The concentration of liquid products depends highly on the mode of operating the the electrochemical reaction. For example, in the zero-gap mode more concentrated products can be obtained than in a flowing electrolyte cell. We will show some sample calculations to estimate the concentrations of ethanol and acetic acid in different cell configuration. The calculations are based on a current density of 500 mA/cm^2 and a Faraday efficiency of 50% for ethylene, 20% for ethanol, 20% for acetic acid, and 10% for hydrogen. From these assumptions and the constraint that we need to convert 10 ton/h of CO_2 to C_2 products (for which an electrolyzer area of 7308 m^2 is required), it is possible to calculate the production rate of ethanol (6.3 mol/s) and acetic acid (9.5 mol/s). The concentration of both products now depends on the supply rate of water to the cathode compartment. In lab experiments, typically a water flow of 0.01–2 ml/min·cm^2 is used. For 0.01, 0.1, and 1 ml/min·cm^2, an ethanol concentration of respectively 0.9%, 0.09%, and 0.009% is obtained. It is clear that low concentration of ethanol will be obtained in a cell with flowing electrolytes.

In the zero-gap mode higher concentration can be obtained, because very low amounts of water are supplied to the cathode. The amount of water in saturated CO_2 can be obtained from the equilibrium relations:[52]

$$y_{\mathrm{CO_2}} P = x_{\mathrm{CO_2}} H_{\mathrm{CO_2}} \quad \text{(Henry's law)} \tag{S17}$$

$$y_w = x_w P_w^{\mathrm{sat.}} \quad \text{(Raoult's law)} \tag{S18}$$

where P is the total pressure, $H_{\mathrm{CO_2}}$ the Henry constant of CO_2 in water, $y_{\mathrm{CO_2}}$ and y_w the gas phase composition of CO_2 and water, $x_{\mathrm{CO_2}}$ and x_w the liquid phase composition of CO_2 and water, and $P_w^{\mathrm{sat.}}$ the saturated vapor pressure of water. The Henry constant of CO_2 in water as a function of temperature is taken from the literature:[53]

$$\ln(H_{\mathrm{CO_2}}/\mathrm{MPa}) = -6.8346 + \frac{1.2817 \cdot 10^4}{T} + \frac{3.7668 \cdot 10^6}{T^2} + \frac{2.997 \cdot 10^8}{T^3} \tag{S19}$$

where the Henry constant is in MPa and the temperature in Kelvin. The saturated vapor pressure of water is obtained from the Antoine equation:[54]

$$P_w^{\text{sat.}} = 10^{A - \frac{B}{C+T}} \tag{S20}$$

where $P_w^{\text{sat.}}$ is in mmHg (760 mmHg = 101.325 kPa) and T in °C. The constant A, B, and C are 8.07131, 1730.63, and 233.426, respectively.[55] By combining the equilibrium relations and setting the total pressure to 1 bar, one can obtain the solubility of CO_2 in water (x_{CO_2}):

$$y_{CO_2} P + y_w P = x_{CO_2} H_{CO_2} + x_w P_w^{\text{sat.}} \tag{S21}$$

In this equation the only unknown is x_{CO_2}, since ($y_{CO_2} + y_w = 1$) and $x_w = (1 - x_{CO_2})$. The amount of water in the gas phase can then be obtained from Raoult's law. The composition of water in the gas phase at 25 °C is around $2.1{\cdot}10^{-5}$ mole fraction. Thus, $2.1{\cdot}10^{-5}$ moles of water per mole of CO_2 is supplied to the cathode. If we assume that this amount of water will mix with the produced ethanol, then the ethanol concentration will be very high (>99.9%). In practice, such a high ethanol concentration is not achieved in zero-gap electrolyzers due to water transport from the anolyte to the catholyte, which dilutes the product stream. To calculate the ethanol concentration accurately, a more complex water balance of the cathode compartment should be solved. The transport of water due to electro-osmotic drag and diffusion, and consumption of water due to electrochemical reactions need to be considered.

The concentration of acetic acid depends on the flow rate of water in the center compartment of the 3-compartment cell. At a current density of 500 mA/cm^2 and a Faraday efficiency of 20%, around 9.5 mol/s of acetate is produced. Therefore, the water flow in the center compartment should be around 2.3 kg/s to obtain 20 wt% of acetic acid. Note that we have assumed that all acetate produced in the cathode compartment is transported to the center compartment.

S7 Loss of CO_2 to (Bi)carbonate

The amount of CO_2 that is lost due to (bi)carbonate formation is estimated from the OH^- generation. We have assumed that all OH^- generated in the CO2RR and water reduction will react with CO_2 to produce (bi)carbonate.

$$2CO_2 + 8H_2O + 12e^- \leftrightarrow C_2H_4 + 12OH^- \tag{S22}$$

$$2CO_2 + 9H_2O + 12e^- \leftrightarrow C_2H_5OH + 12OH^- \tag{S23}$$

$$2CO_2 + 6H_2O + 8e^- \leftrightarrow CH_3COOH + 8OH^- \tag{S24}$$

$$2H_2O + 2e^- \leftrightarrow H_2 + 2OH^- \tag{S25}$$

For every mole of ethylene, ethanol, acetic acid, and hydrogen 12, 12, 8, and 2 moles of hydroxide ions are produced. The hydroxide ions will react with CO_2:

$$CO_2 + OH^- \leftrightarrow HCO_3^- \tag{S26}$$

For a current density of 500 mA/cm^2 and a Faraday efficiency of 50% for ethylene, 20% for ethanol, 20% for acetic acid, and 10% for hydrogen, 6 times more CO_2 (60 ton/h) is lost than electrochemically converted (10 ton/h) to C_2 products. It is clear that the cost of CO_2 will increase dramatically if the CO2RR is performed in alkaline media. Note that we have only accounted for CO_2 reactions with the hydroxides generated from the electrochemical reduction of CO_2 and water. More CO_2 will be lost if an alkaline catholyte (e.g., KOH) is used. In the process design, we have assumed that all the lost CO_2 (in the form of (bi)carbonate) can be regenerated in the center compartment of a 3-compartment cell.

References

(1) García de Arquer, F. P.; Dinh, C.-T.; Ozden, A.; Wicks, J.; McCallum, C.; Kirmani, A. R.; Nam, D.-H.; Gabardo, C.; Seifitokaldani, A.; Wang, X.; Li, Y. C.; Li, F.; Edwards, J.; Richter, L. J.; Thorpe, S. J.; Sinton, D.; Sargent, E. H. CO_2 electrolysis to multicarbon products at activities greater than 1 A cm^{-2}. *Science* **2020**, *367*, 661–666.

(2) Dinh, C.-T.; Burdyny, T.; Kibria, M. G.; Seifitokaldani, A.; Gabardo, C. M.; García de Arquer, F. P.; Kiani, A.; Edwards, J. P.; De Luna, P.; Bushuyev, O. S.; Zou, C.; Quintero-Bermudez, R.; Pang, Y.; Sinton, D.; Sargent, E. H. CO_2 electroreduction to ethylene via hydroxide-mediated copper catalysis at an abrupt interface. *Science* **2018**, *360*, 783–787.

(3) De Gregorio, G. L.; Burdyny, T.; Loiudice, A.; Iyengar, P.; Smith, W. A.; Buonsanti, R. Facet-Dependent Selectivity of Cu Catalysts in Electrochemical CO_2 Reduction at Commercially Viable Current Densities. *ACS Catal.* **2020**, *10*, 4854–4862.

(4) Hoang, T. T. H.; Verma, S.; Ma, S.; Fister, T. T.; Timoshenko, J.; Frenkel, A. I.; Kenis, P. J. A.; Gewirth, A. A. Nanoporous Copper–Silver Alloys by Additive-Controlled Electrodeposition for the Selective Electroreduction of CO_2 to Ethylene and Ethanol. *J. Am. Chem. Soc.* **2018**, *140*, 5791–5797.

(5) Vennekötter, J.-B.; Scheuermann, T.; Sengpiel, R.; Wessling, M. The electrolyte matters: Stable systems for high rate electrochemical CO_2 reduction. *J. CO2 Util.* **2019**, *32*, 202–213.

(6) Wang, X.; Wang, Z.; García de Arquer, F. P.; Dinh, C.-T.; Ozden, A.; Li, Y. C.; Nam, D.-H.; Li, J.; Liu, Y.-S.; Wicks, J.; Chen, Z.; Chi, M.; Chen, B.; Wang, Y.; Tam, J.; Howe, J. Y.; Proppe, A.; Todorović, P.; Li, F.; Zhuang, T.-T.; Gabardo, C. M.; Kirmani, A. R.; McCallum, C.; Hung, S.-F.; Lum, Y.; Luo, M.; Min, Y.; Xu, A.;

O'Brien, C. P.; Stephen, B.; Sun, B.; Ip, A. H.; Richter, L. J.; Kelley, S. O.; Sinton, D.; Sargent, E. H. Efficient electrically powered CO_2-to-ethanol via suppression of deoxygenation. *Nat. Energy* **2020**, *5*, 478–486.

(7) Zhong, M.; Tran, K.; Min, Y.; Wang, C.; Wang, Z.; Dinh, C.-T.; De Luna, P.; Yu, Z.; Rasouli, A. S.; Brodersen, P.; Sun, S.; Voznyy, O.; Tan, C.-S.; Askerka, M.; Che, F.; Liu, M.; Seifitokaldani, A.; Pang, Y.; Lo, S.-C.; Ip, A.; Ulissi, Z.; Sargent, E. H. Accelerated discovery of CO_2 electrocatalysts using active machine learning. *Nature* **2020**, *581*, 178–183.

(8) Chen, X.; Chen, J.; Alghoraibi, N. M.; Henckel, D. A.; Zhang, R.; Nwabara, U. O.; Madsen, K. E.; Kenis, P. J. A.; Zimmerman, S. C.; Gewirth, A. A. Electrochemical CO_2-to-ethylene conversion on polyamine-incorporated Cu electrodes. *Nat. Catal.* **2021**, *4*, 20–27.

(9) Li, F.; Thevenon, A.; Rosas-Hernández, A.; Wang, Z.; Li, Y.; Gabardo, C. M.; Ozden, A.; Dinh, C. T.; Li, J.; Wang, Y.; Edwards, J. P.; Xu, Y.; McCallum, C.; Tao, L.; Liang, Z.-Q.; Luo, M.; Wang, X.; Li, H.; O'Brien, C. P.; Tan, C.-S.; Nam, D.-H.; Quintero-Bermudez, R.; Zhuang, T.-T.; Li, Y. C.; Han, Z.; Britt, R. D.; Sinton, D.; Agapie, T.; Peters, J. C.; Sargent, E. H. Molecular tuning of CO_2-to-ethylene conversion. *Nature* **2020**, *577*, 509–513.

(10) Ma, W.; Xie, S.; Liu, T.; Fan, Q.; Ye, J.; Sun, F.; Jiang, Z.; Zhang, Q.; Cheng, J.; Wang, Y. Electrocatalytic reduction of CO_2 to ethylene and ethanol through hydrogen-assisted C–C coupling over fluorine-modified copper. *Nat. Catal.* **2020**, *3*, 478–487.

(11) Ozden, A.; Li, F.; Garcia de Arquer, F. P.; Rosas-Hernández, A.; Thevenon, A.; Wang, Y.; Hung, S.-F.; Wang, X.; Chen, B.; Li, J.; Wicks, J.; Luo, M.; Wang, Z.; Agapie, T.; Peters, J. C.; Sargent, E. H.; Sinton, D. High-Rate and Efficient Ethylene

Electrosynthesis Using a Catalyst/Promoter/Transport Layer. *ACS Energy Lett.* **2020**, *5*, 2811–2818.

(12) She, X.; Zhang, T.; Li, Z.; Li, H.; Xu, H.; Wu, J. Tandem Electrodes for Carbon Dioxide Reduction into C2+ Products at Simultaneously High Production Efficiency and Rate. *Cell Reports Phys. Sci.* **2020**, *1*, 100051.

(13) Tan, Y. C.; Lee, K. B.; Song, H.; Oh, J. Modulating Local CO_2 Concentration as a General Strategy for Enhancing C-C Coupling in CO_2 Electroreduction. *Joule* **2020**, *4*, 1104–1120.

(14) Wang, Y.; Wang, Z.; Dinh, C.-T.; Li, J.; Ozden, A.; Golam Kibria, M.; Seifitokaldani, A.; Tan, C.-S.; Gabardo, C. M.; Luo, M.; Zhou, H.; Li, F.; Lum, Y.; McCallum, C.; Xu, Y.; Liu, M.; Proppe, A.; Johnston, A.; Todorovic, P.; Zhuang, T.-T.; Sinton, D.; Kelley, S. O.; Sargent, E. H. Catalyst synthesis under CO_2 electroreduction favours faceting and promotes renewable fuels electrosynthesis. *Nat. Catal.* **2020**, *3*, 98–106.

(15) Romero Cuellar, N.; Wiesner-Fleischer, K.; Fleischer, M.; Rucki, A.; Hinrichsen, O. Advantages of CO over CO_2 as reactant for electrochemical reduction to ethylene, ethanol and n-propanol on gas diffusion electrodes at high current densities. *Electrochim. Acta* **2019**, *307*, 164–175.

(16) Romero Cuellar, N.; Scherer, C.; Kaçkar, B.; Eisenreich, W.; Huber, C.; Wiesner-Fleischer, K.; Fleischer, M.; Hinrichsen, O. Two-step electrochemical reduction of CO_2 towards multi-carbon products at high current densities. *J. CO2 Util.* **2020**, *36*, 263–275.

(17) Jouny, M.; Luc, W.; Jiao, F. High-rate electroreduction of carbon monoxide to multicarbon products. *Nat. Catal.* **2018**, *1*, 748–755.

(18) Jouny, M.; Lv, J.-J.; Cheng, T.; Ko, B. H.; Zhu, J.-J.; Goddard, W. A.; Jiao, F. Formation of carbon–nitrogen bonds in carbon monoxide electrolysis. *Nat. Chem.* **2019**, *11*, 846–851.

(19) Li, J.; Wang, Z.; McCallum, C.; Xu, Y.; Li, F.; Wang, Y.; Gabardo, C. M.; Dinh, C.-t.; Zhuang, T.-t.; Wang, L.; Howe, J. Y.; Ren, Y.; Sargent, E. H.; Sinton, D. Constraining CO coverage on copper promotes high-efficiency ethylene electroproduction. *Nat. Catal.* **2019**, *2*, 1124–1131.

(20) Luc, W.; Fu, X.; Shi, J.; Lv, J.-J.; Jouny, M.; Ko, B. H.; Xu, Y.; Tu, Q.; Hu, X.; Wu, J.; Yue, Q.; Liu, Y.; Jiao, F.; Kang, Y. Two-dimensional copper nanosheets for electrochemical reduction of carbon monoxide to acetate. *Nat. Catal.* **2019**, *2*, 423–430.

(21) Ozden, A.; Wang, Y.; Li, F.; Luo, M.; Sisler, J.; Thevenon, A.; Rosas-Hernández, A.; Burdyny, T.; Lum, Y.; Yadegari, H.; Agapie, T.; Peters, J. C.; Sargent, E. H.; Sinton, D. Cascade CO_2 electroreduction enables efficient carbonate-free production of ethylene. *Joule* **2021**, *5*, 706–719.

(22) Ren, S.; Fink, A. G.; Lees, E. W.; Zhang, Z.; Wu, W.; Dvorak, D. J. Molecular electrocatalysts transform CO into C2+ products effectively in a flow cell. *Researchsquare.Com* **2020**, 1–18.

(23) Ripatti, D. S.; Veltman, T. R.; Kanan, M. W. Carbon Monoxide Gas Diffusion Electrolysis that Produces Concentrated C_2 Products with High Single-Pass Conversion. *Joule* **2019**, *3*, 240–256.

(24) Zhu, P.; Xia, C.; Liu, C.-Y.; Jiang, K.; Gao, G.; Zhang, X.; Xia, Y.; Lei, Y.; Alshareef, H. N.; Senftle, T. P.; Wang, H. Direct and continuous generation of pure acetic acid solutions via electrocatalytic carbon monoxide reduction. *Proc. Natl. Acad. Sci.* **2021**, *118*, e2010868118.

(25) Jeanty, P.; Scherer, C.; Magori, E.; Wiesner-Fleischer, K.; Hinrichsen, O.; Fleischer, M. Upscaling and continuous operation of electrochemical CO_2 to CO conversion in aqueous solutions on silver gas diffusion electrodes. *J. CO2 Util.* **2018**, *24*, 454–462.

(26) Duarte, M.; De Mot, B.; Hereijgers, J.; Breugelmans, T. Electrochemical Reduction of CO_2 : Effect of Convective CO_2 Supply in Gas Diffusion Electrodes. *ChemElectroChem* **2019**, *6*, 5596–5602.

(27) Endrődi, B.; Kecsenovity, E.; Samu, A.; Darvas, F.; Jones, R. V.; Török, V.; Danyi, A.; Janáky, C. Multilayer Electrolyzer Stack Converts Carbon Dioxide to Gas Products at High Pressure with High Efficiency. *ACS Energy Lett.* **2019**, *4*, 1770–1777.

(28) Dinh, C.-T.; García de Arquer, F. P.; Sinton, D.; Sargent, E. H. High Rate, Selective, and Stable Electroreduction of CO_2 to CO in Basic and Neutral Media. *ACS Energy Lett.* **2018**, *3*, 2835–2840.

(29) Dufek, E. J.; Lister, T. E.; Stone, S. G.; McIlwain, M. E. Operation of a Pressurized System for Continuous Reduction of CO_2. *J. Electrochem. Soc.* **2012**, *159*, F514–F517.

(30) Haas, T.; Krause, R.; Weber, R.; Demler, M.; Schmid, G. Technical photosynthesis involving CO_2 electrolysis and fermentation. *Nat. Catal.* **2018**, *1*, 32–39.

(31) Ma, S.; Luo, R.; Gold, J. I.; Yu, A. Z.; Kim, B.; Kenis, P. J. A. Carbon nanotube containing Ag catalyst layers for efficient and selective reduction of carbon dioxide. *J. Mater. Chem. A* **2016**, *4*, 8573–8578.

(32) Wang, R.; Haspel, H.; Pustovarenko, A.; Dikhtiarenko, A.; Russkikh, A.; Shterk, G.; Osadchii, D.; Ould-Chikh, S.; Ma, M.; Smith, W. A.; Takanabe, K.; Kapteijn, F.; Gascon, J. Maximizing Ag Utilization in High-Rate CO_2 Electrochemical Reduction with a Coordination Polymer-Mediated Gas Diffusion Electrode. *ACS Energy Lett.* **2019**, *4*, 2024–2031.

(33) Salvatore, D. A.; Weekes, D. M.; He, J.; Dettelbach, K. E.; Li, Y. C.; Mallouk, T. E.; Berlinguette, C. P. Electrolysis of Gaseous CO_2 to CO in a Flow Cell with a Bipolar Membrane. *ACS Energy Lett.* **2018**, *3*, 149–154.

(34) Edwards, J. P.; Xu, Y.; Gabardo, C. M.; Dinh, C.-T.; Li, J.; Qi, Z.; Ozden, A.; Sargent, E. H.; Sinton, D. Efficient electrocatalytic conversion of carbon dioxide in a low-resistance pressurized alkaline electrolyzer. *Appl. Energy* **2020**, *261*, 114305.

(35) Reinisch, D.; Schmid, B.; Martić, N.; Krause, R.; Landes, H.; Hanebuth, M.; Mayrhofer, K. J.; Schmid, G. Various CO_2-to-CO Electrolyzer Cell and Operation Mode Designs to avoid CO_2-Crossover from Cathode to Anode. *Zeitschrift für Phys. Chemie* **2020**, *234*, 1115–1131.

(36) Bhargava, S. S.; Proietto, F.; Azmoodeh, D.; Cofell, E. R.; Henckel, D. A.; Verma, S.; Brooks, C. J.; Gewirth, A. A.; Kenis, P. J. A. System Design Rules for Intensifying the Electrochemical Reduction of CO_2 to CO on Ag Nanoparticles. *ChemElectroChem* **2020**, *7*, 2001–2011.

(37) Lee, W. H.; Ko, Y.-J.; Choi, Y.; Lee, S. Y.; Choi, C. H.; Hwang, Y. J.; Min, B. K.; Strasser, P.; Oh, H.-S. Highly selective and scalable CO_2 to CO - Electrolysis using coral-nanostructured Ag catalysts in zero-gap configuration. *Nano Energy* **2020**, *76*, 105030.

(38) Lee, J.; Lee, W.; Ryu, K. H.; Park, J.; Lee, H.; Lee, J. H.; Park, K. T. Catholyte-free electroreduction of CO_2 for sustainable production of CO: concept, process development, techno-economic analysis, and CO_2 reduction assessment. *Green Chem.* **2021**, *23*, 2397–2410.

(39) Kaczur, J. J.; Yang, H.; Liu, Z.; Sajjad, S. D.; Masel, R. I. Carbon Dioxide and Water Electrolysis Using New Alkaline Stable Anion Membranes. *Front. Chem.* **2018**, *6*, 1–16.

(40) Liu, Z.; Yang, H.; Kutz, R.; Masel, R. I. CO_2 Electrolysis to CO and O_2 at High Selectivity, Stability and Efficiency Using Sustainion Membranes. *J. Electrochem. Soc.* **2018**, *165*, J3371–J3377.

(41) Verma, S.; Hamasaki, Y.; Kim, C.; Huang, W.; Lu, S.; Jhong, H.-R. M.; Gewirth, A. A.; Fujigaya, T.; Nakashima, N.; Kenis, P. J. A. Insights into the Low Overpotential Electroreduction of CO_2 to CO on a Supported Gold Catalyst in an Alkaline Flow Electrolyzer. *ACS Energy Lett.* **2018**, *3*, 193–198.

(42) Endrődi, B.; Kecsenovity, E.; Samu, A.; Halmágyi, T.; Rojas-Carbonell, S.; Wang, L.; Yan, Y.; Janáky, C. High carbonate ion conductance of a robust PiperION membrane allows industrial current density and conversion in a zero-gap carbon dioxide electrolyzer cell. *Energy Environ. Sci.* **2020**, *13*, 4098–4105.

(43) Endrődi, B.; Samu, A.; Kecsenovity, E.; Halmágyi, T.; Sebők, D.; Janáky, C. Operando cathode activation with alkali metal cations for high current density operation of water-fed zero-gap carbon dioxide electrolysers. *Nat. Energy* **2021**, *6*, 439–448.

(44) Pettersen, T.; Lien, K. A new robust design model for gas separating membrane modules, based on analogy with counter-current heat exchangers. *Comput. Chem. Eng.* **1994**, *18*, 427–439, An International Journal of Computer Applications in Chemical Engineering.

(45) Al-Rabiah, a. a.; Timmerhaus, K. D.; Noble, R. D. Membrane Technology for Hydrogen Separation in Ethylene Plants. 6th World Congr. Chem. Eng. Melbourne, 2001; pp 1–7.

(46) Xiao, P.; Zhang, J.; Webley, P.; Li, G.; Singh, R.; Todd, R. Capture of CO_2 from flue gas streams with zeolite 13X by vacuum-pressure swing adsorption. *Adsorption* **2008**, *14*, 575–582.

(47) Choi, B.-U.; Choi, D.-K.; Lee, Y.-W.; Lee, B.-K.; Kim, S.-H. Adsorption Equilibria of

Methane, Ethane, Ethylene, Nitrogen, and Hydrogen onto Activated Carbon. *J. Chem. Eng. Data* **2003**, *48*, 603–607.

(48) Luyben, W. L. Capital cost of compressors for conceptual design. *Chemical Engineering and Processing - Process Intensification* **2018**, *126*, 206–209.

(49) Shah, V. H.; Pham, V.; Larsen, P.; Biswas, S.; Frank, T. Liquid–Liquid Extraction for Recovering Low Margin Chemicals: Thinking beyond the Partition Ratio. *Ind. Eng. Chem. Res.* **2016**, *55*, 1731–1739.

(50) Todd, D. B. *Ferment. Biochem. Eng. Handb.*, 2nd ed.; Elsevier, 2014; pp 225–238.

(51) Woods, D. R. *Rules of Thumb in Engineering Practice*; Wiley-VCH Verlag GmbH & Co. KGaA: Weinheim, Germany, 2007; pp 376–436.

(52) Smith, J.; Van Ness, H.; Abbott, M. *Introduction to Chemical Engineering Thermodynamics*, seventh ed.; CHEMICAL ENGINEERING SERIES; McGraw-Hill Education: New York, 2005.

(53) Carroll, J. J.; Slupsky, J. D.; Mather, A. E. The Solubility of Carbon Dioxide in Water at Low Pressure. *J. Phys. Chem. Ref. Data* **1991**, *20*, 1201–1209.

(54) Prausnitz, J.; Lichtenthaler, R.; Gomes de Azevedo, E. *Molecular thermodynamics of fluid-phase equilibria*, 3rd ed.; Prentice Hall PTR: New York, 1999.

(55) Dortmund Data Bank, url = www.ddbst.com, note = Accessed: 2021-08-01.